International Journal of Biological Macromolecules 377 (2026) 153600

Contents lists available at ScienceDirect

International Journal of Biological Macromolecules

journal homepage: www.elsevier.com/locate/ijbiomac

Encapsulation of quercetin in pullulan-coated zein nanoparticles

Jialin Sun [a], Megan Povey [a], Wing-Fu Lai [a], Paraskevi Paximada [a,*]

[a] School of Food Science and Nutrition, Faculty of Environment, University of Leeds, Leeds, LS2 9JT, United Kingdom

ARTICLE INFO

Keywords:
Nanoparticle
Zein
Pullulan
Quercetin
Encapsulation

ABSTRACT

Quercetin (Que), a natural flavonoid with high antioxidant activity, exhibits limited application in aqueous systems due to its poor water solubility and instability. To address these limitations, this study developed and characterized zein-pullulan composite nanoparticles for the encapsulation and protection of Que. Zein nanoparticles (Z NPs) and Que-loaded zein nanoparticles (ZQ NPs) were first prepared via antisolvent-induced self-assembly, employing hydrophobic interactions and hydrogen bonding. Subsequently, pullulan (PUL), a hydrophilic and biodegradable polysaccharide, was deposited onto the surface of Z NPs and ZQ NPs through electrostatic interaction to form ZP NPs and ZQP NPs. The optimized ZQP NPs exhibited a core-shell structure with high encapsulation efficiency and spherical morphology. Surface coating with PUL significantly enhanced the hydrophilicity of the nanoparticles, as confirmed by water contact angle measurements, and also enhanced their thermal and storage stability. After 12 days of storage at 4 °C, ZQP NPs maintained the highest Que retention rate of 88.10 ± 0.16%. Additionally, both ZQ NPs and ZQP NPs showed strong antioxidant ability. These results demonstrate that zein-pullulan composite nanoparticles are a promising antioxidant delivery system, offering both protection and aqueous compatibility for hydrophobic bioactives, and suggesting great potential for incorporation into water-soluble antioxidant films.

1. Introduction

Flavonoids can be found in various plants, including vegetables, flowers, fruits, and tea leaves. Quercetin (Que), a flavonoid, exhibits a variety of biological activities such as antioxidant, anti-inflammatory, and antimicrobial [1,2]. These activities can be beneficial for human health by reducing oxidative stress, inflammation, and microbial infections, while also improving food quality and safety by delaying oxidation and inhibiting the growth of spoilage and microorganisms [3,4]. However, the use of Que has been severely constrained due to its chemical structure. The chemical structure of Que features a parent skeleton composed of three benzene rings (A, B, and C rings), forming a planar conjugated system. This fused aromatic structure exhibits pronounced hydrophobicity, which impedes its interaction with polar water molecules and results in low solubility in aqueous system [5,6]. These characteristics limit the use of Que in water-soluble matrices. Moreover, Que is susceptible to oxidation and light, which has an effect on its biological activities [7–9]. Therefore, it is of importance to find a method to both protect Que and improve its usage in water-soluble matrices.

In recent years, with the development of nanotechnology, nano encapsulation has been confirmed to be a potential strategy for the protection of bioactive. Nanoencapsulation is considered an effective strategy for improving the delivery of hydrophobic bioactive compounds such as quercetin. It can enhance aqueous dispersibility, improve physicochemical stability, and protect sensitive compounds from degradation during processing and storage. Therefore, nanoencapsulation has attracted increasing attention as a promising approach for overcoming the poor water solubility and instability of quercetin. Various delivery systems have been developed for quercetin, including emulsions, nanoparticles, and liposomes. Emulsion carriers might enhance the dispersibility of lipophilic Que in aqueous formulations. However, they typically use surfactants and are unstable systems. Their main physical destabilization mechanisms include coalescence and Ostwald ripening during emulsification and storage [10]. Liposomes offer a biocompatible bilayer for Que incorporation, yet long-term application can be constrained by issues such as payload leakage, aggregation or rupture under harsh pH or elevated temperature, and phospholipid oxidation, which may compromise stability in aqueous matrices [11,12]. Spray drying provides a scalable route to convert Que formulations into dry powders. Nevertheless, exposure to heated air and high-energy atomization may cause thermal degradation of Que during

* Corresponding author.
E-mail address: E.Paximada@leeds.ac.uk (P. Paximada).

https://doi.org/10.1016/j.ijbiomac.2026.153600
Received 17 February 2026; Received in revised form 2 July 2026; Accepted 16 July 2026
Available online 17 July 2026

processing [5,13]. Therefore, nanoparticles are increasingly considered as a promising solution because they can offer stronger protection against oxygen and light, improved aqueous dispersibility, and achieve sustained release of Que [14].

To improve the stability of Que, various carrier systems have been explored. For example, Hassan et al. [15] developed a protein/polysaccharide-based delivery system using pectin, zein, and β-cyclodextrin to encapsulate Que, and found that the concentration of Que remained unchanged for up to two weeks at 4 °C. These results indicate that carrier-assisted delivery is an effective strategy for improving the stability of Que. Among the different carrier materials investigated, proteins are regarded as particularly promising due to their wide sources, good biocompatibility, and excellent delivery performance [16]. Among them, zein is especially attractive because of its amphiphilic nature and strong potential for encapsulating hydrophobic bioactive compounds [17]. The hydrophobicity of zein enables self-assembly into nanoparticles via the antisolvent method, thereby simplifying both the nanoparticle formation process and the kinetic driving mechanisms. The anti-solvent method is widely used for nanoparticle preparation because the decrease in solvent quality can induce zein self-assembly into nanoparticles. In addition, this method is simple, mild, and suitable for encapsulating hydrophobic compounds. Previous studies have been conducted on zein-based nanoparticle fabrication, encompassing the encapsulation and delivery of diverse bioactive nutrients, such as ferulic acid, curcumin, and cinnamaldehyde [18–20]. Despite this, the hydrophobicity of zein restricts its use in hydrophilic systems and might result in destabilization. Polysaccharide incorporation is thus widely adopted to stabilize particles in aqueous dispersion.

Representative examples include soluble soybean polysaccharide, xanthan gum, and other negatively charged biopolymers, which have been used to stabilize zein-based nanoparticles mainly by improving colloidal stability, encapsulation, and delivery performance of hydrophobic bioactives. However, for the present study, pullulan was selected not only as a hydrophilic coating polysaccharide, but also because of its particular relevance to food packaging applications [21–24]. Pullulan (PUL) is a water-soluble, exopolysaccharide produced by fungal fermentation by *Aureobasidium pullulans*. This linear glucan consists predominantly of maltotriose units interconnected via α-(1 → 6) glycosidic linkages, creating a unique alternating pattern of α-(1 → 4) and α-(1 → 6) bonds. Its distinctive molecular structure offers high flexibility and adhesiveness, and remarkable oxygen barrier capacity [25,26]. Meanwhile, it is also classified as GRAS by the United States Food and Drug Administration (US-FDA).

Polysaccharides are typically negatively charged, meaning that electrostatic interactions can be used to accelerate the deposition of polysaccharides on the surface of protein nanoparticles, thus achieving the improvement of pH, ionic, and storage stability [27]. Due to the hydrophilicity of pullulan, compared with a generic stabilizing polysaccharide layer, a pullulan coating was expected to provide a hydrated surface layer for improving the dispersibility and storage stability of zein/quercetin nanoparticles, while also offering better compatibility with future incorporation into active packaging matrices. Notably, the encapsulated Que retains its intrinsic antioxidant activity within the nanoparticle matrix, creating an integrated antioxidant delivery platform with the dual functionality of carrier and active compounds.

Hence, the aim of this study is to develop and characterize quercetin-loaded zein-pullulan composite nanoparticles (ZQP NPs) as a promising antioxidant delivery system for future food packaging applications. Meanwhile, Que was used as a packaging-relevant model antioxidant vehicle to evaluate whether the proposed nanoparticle system could improve its water compatibility and storage-related stability. Firstly, zein and Que-loaded zein nanoparticles (Z NPs and ZQ NPs) were produced with self-assembly by hydrophobic interactions and hydrogen bonding. To further enhance the stability and surface properties of the nanoparticles, pullulan (PUL) was coated onto the Z NPs and ZQ NPs via electrostatic interaction and hydrogen bonding, to form ZP NPs and ZQP NPs. The physicochemical properties together with the storage stability have been evaluated. The significance of this study lies in evaluating PUL as a packaging-relevant coating material for the construction of ZQP NPs intended for future active food packaging applications. This study provides insight into the development of stable and water-compatible antioxidant nanocarriers and lays a foundation for their further application in functional water-soluble antioxidant films.

2. Materials and methods

2.1. Materials

Zein powder (Source: SLCN6870; CAS number: 9010-66-6) was purchased from Sigma-Aldrich (USA). Pullulan (Mw 362–480 kDa, Cat#HY-W1–45522) was obtained from Cambridge Bioscience (Cambridge, UK). Quercetin with purity ≥95% and 2,2-Diphenyl-1-picrylhydrazyl (DPPH) were purchased from Sigma-Aldrich (USA), while ethanol absolute (≥99.5%) was purchased from WVR Chemicals (Leicestershire, UK). All reagents were of analytical grade.

2.2. Preparation of zein nanoparticles (Z NPs) and zein/pullulan nanoparticles (ZP NPs)

The preparation process and schematic diagram of formation of Z NPs and ZQ NPs are illustrated in Fig. 1. The tested mass ratios of zein to pullulan ranged from 3:1 to 1:10, and the corresponding sample abbreviations are summarized in *Supplementary Material* Table S1. Briefly, 2% *w/v* Zein was dispersed in 70% *v*/v ethanol and pullulan was dissolved in deionized water at concentrations of 0.066%, 0.1%, 0.2%, 0.4%, 0.6%, 1%, and 2% *w/v*, respectively. To form the nanoparticles, zein dispersion was added into deionized water at pH 3.00, 4.00, and 5.00 at a concentration of 0.2% w/v, followed by magnetic stirring at 550 rpm for 2 h. A rotary evaporator (Heizbad Hei-VAP, Heldolph, Germany) was used to remove ethanol at 40 °C to obtain Z NPs aqueous dispersions. Meanwhile, the pH of Z NPs water dispersion solution was adjusted to 3.00, 4.00 and 5.00 for use in subsequent experiments. Pullulan aqueous solution was also adjusted to pH 3.00, 4.00, and 5.00, respectively. Subsequently, Z NPs aqueous dispersions at varying pH values were added to equal volume of pullulan solution at different concentrations for 3 h at 550 rpm to obtain ZP NPs.

2.3. Preparation of que-loaded zein nanoparticles (ZQ NPs) and que-loaded zein/pullulan nanoparticles (ZQP NPs)

Zein (2% *w/v*) and quercetin (0.5, 1.0, 1.5, and 2.0 mg/mL) were fully dissolved simultaneously in 70% *v*/v ethanol in advance. To prepare ZQ NPs, zein-quercetin solution was dropped into deionized water at pH 5.00 and subjected to magnetic stirring at 550 rpm for 2 h. A rotary evaporator was also used to remove ethanol at 40 °C to obtain ZQ NPs aqueous dispersions, and the pH was subsequently adjusted to 5.00. For the formation of ZQP NPs, 0.6% *w/v* pullulan solution at pH 5.00 was mixed with the above ZQ NPs aqueous dispersions with equal volume at 550 rpm for 3 h to ensure complete electrostatic deposition. The analysis was performed using the fresh sample, unless otherwise stated.

2.4. Characterization of nanoparticles

2.4.1. Physical properties

Measurements of ζ potential, particle size, and polydispersity index (PDI) were carried out by Zetasizer (ZEN3600, Malvern, UK) at 25 °C.

The turbidity of ZP NPs was characterized at 600 nm by a UV/Vis. Spectrophotometer (6715, JENWAY, UK), and deionized water was used as blank.

2.4.2. Encapsulation efficiency (EE) and loading capacity (LC) of Que

The freshly prepared ZQ NPs and ZQP NPs aqueous dispersions were

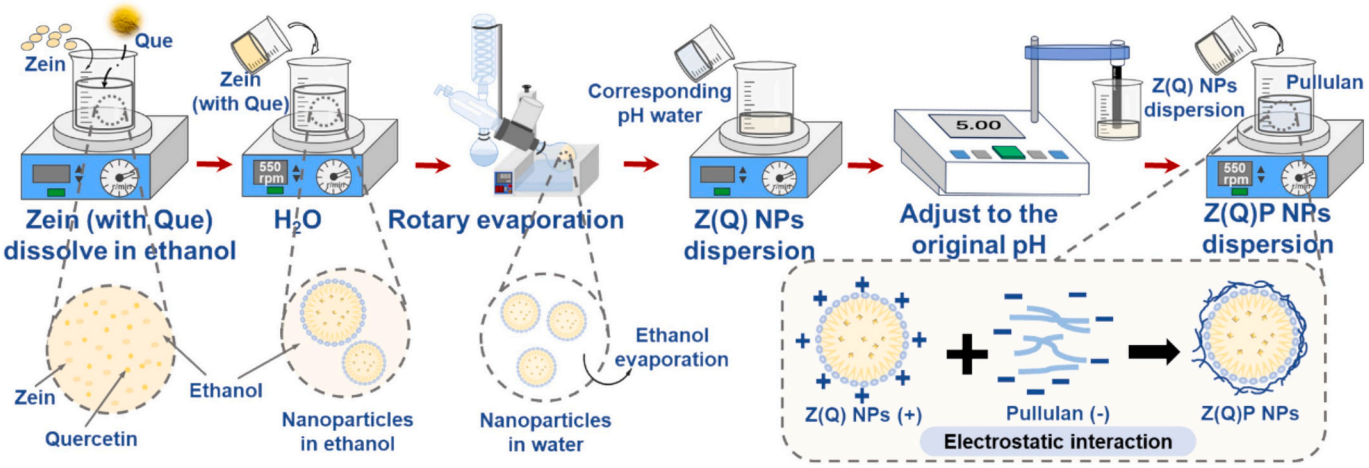

Fig. 1. Schematic illustration of the preparation procedure and proposed formation mechanism of Z(Q) NPs and Z(Q)P NPs.

centrifuged at 12,000 rpm under 4 °C for 20 min to collect supernatant. A UV/Vis. Spectrophotometer (6715, JENWAY, UK) was employed to evaluate the absorbance of supernatant at 370 nm to determine the unencapsulated Que concentration according to the established standard calibration curve of Que. The EE and LC were calculated by Eqs. (1) and (2).

$$\text{EE}\ (\%) = \frac{\textit{Total Que} - \textit{Free Que}}{\textit{Total Que}} \times 100\% \tag{1}$$

$$\text{LC}\ (\%) = \frac{W_{\text{encapsulated Que}}}{W_{\text{nanoparticles}} + W_{\text{encapsulated Que}}} \times 100\% \tag{2}$$

where, total Que and free Que referred to the mass of quercetin initially added and unencapsulated by nanoparticles, respectively. $W_{\text{encapsulated Que}}$ and $W_{\text{nanoparticles}}$ referred to the mass of Que encapsulated and the Que-loaded nanoparticles, respectively.

2.4.3. Surface morphology

The surface morphology was determined by scanning electron microscopy (SEM) (SU8230, Hitachi, Japan) with an accelerating voltage of 2 kV. Carbon spraying was implemented in advance to achieve surface observation.

As for TEM analysis, freshly prepared dispersions of Z NPs, ZQ NPs, and ZQP NPs were dropped onto carbon-coated TEM grids and dried at room temperature before observation. The morphology and structural features of nanoparticles were examined using a transmission electron microscopy (TEM) (FEI Titan Cubed Themis 300 G2 FEG STEM, Thermo Fisher Scientific, USA) at 300 kV.

2.4.4. Attenuated total reflectance-fourier transform infrared (ATR-FTIR) spectrum analysis

Nanoparticles obtained by freeze-drying were used for ATR-FTIR (VERTEX 80v, Bruker, Germany). The spectrum was recorded with a wavenumber range from 4000 cm^{-1} to 650 cm^{-1}, with 64 scans at a resolution of 4 cm^{-1}.

2.4.5. Water contact angle (WCA)

The powder obtained by freeze-drying was compressed into thin sheets by applying 10 MPa through a hydraulic press (CSA10BB, Clarke, UK) [28]. Subsequently, a Drop Shape Tensiometer (OCA 25, dataphysics, Germany) was used to determine the interfacial hydrophilicity or hydrophobicity by measuring the three-phase contact angle of thin slices. Among them, rapeseed oil was selected as the oil phase and stored in a container, while the slices were immersed in the oil. Deionized water was dripped onto the surface of the thin slice, and after waiting for three minutes, photos were taken to record the WCA.

2.4.6. Thermal stability

The heating treatment at 90 °C was used as an accelerated stress test to evaluate the thermal stability of the nanoparticles under elevated-temperature conditions. This condition was selected with consideration of their potential future incorporation into film-forming systems, in which heating is often applied during solution casting to promote solvent evaporation and film formation. Freshly prepared ZQ NPs and ZQP NPs water dispersion solution were centrifuged at 12,000 rpm under 4 °C for 20 min to remove unloaded Que. The corresponding volume of deionized water was added to the centrifuged precipitate to restore its original volume. Subsequently, solutions were placed in a water bath and heated at 90 °C for 120 mins to determine the thermal stability of the nanoparticles by measuring the content of Que in the nanoparticles. Samples were taken every 20 mins, and the content of Que was measured according to the standard curve of Que at 370 nm. The thermal stability of nanoparticles was calculated through the retention rate of Que.

$$\text{Retention rate}\ (\%) = \frac{\text{Que content after heat treatment}}{\text{Initial actual content of Que}} \tag{3}$$

2.4.7. Storage stability and photostability

To investigate the storage stability of nanoparticles, freshly prepared nanoparticles dispersions were stored at 4 °C for 12 d. The particle sizes of Z NPs, ZQ NPs, ZP NPs and ZQP NPs were measured every three days by Zetasizer (ZEN3600, Malvern, UK) at 25 °C.

For the evaluation of the retention of quercetin during storage, samples were collected at selected time intervals. The ZQ NPs and ZQP NPs dispersions were subjected to centrifugation at 12,000 rpm and 4 °C for 20 min, and the resulting supernatant was collected. The supernatants were measured at 370 nm by a UV/Vis. Spectrophotometer (6715, JENWAY, UK) and the retention rate was calculated according to the Eq. (4).

$$\text{Retention rate}\ (\%) = \frac{\text{Que content after storage}}{\text{Initial actual content of Que}} \tag{4}$$

For the test of photostability, the detailed experimental conditions are described in the *Supplementary Material.*

2.4.8. Antioxidant ability

Considering the varying dispersion of different nanoparticles in different solutions, the nanoparticles were dispersed according to *Supplementary Material* Table S2, and the final concentration of DPPH was 0.025 g/L.

The absorbance of DPPH dissolved in 95% (*v*/v) ethanol was set as blank, and the sample-DPPH mixture was placed in the shaker in the

dark at 25 °C for 30 mins. The absorbance of the solution after the reaction was determined at 517 nm and the free radical scavenging ability was calculated according to the Eq. (5).

$$\text{DPPH scavenging rate } (\%) = \frac{A_{Blank} - A_{Sample}}{A_{Blank}} \times 100\% \quad (5)$$

where A_{Black} and A_{Sample} were the absorbance of DPPH solution and mixtures of DPPH and label extracts at 517 nm, respectively.

To provide a more application-relevant evaluation of antioxidant activity, the ABTS radical scavenging activity of all samples was further determined in 10% *v*/v ethanol food simulant. ABTS solution was prepared using 7.4 mmol/L ABTS and 2.6 mmol/L potassium persulfate ($K_2S_2O_8$) stock solution. All samples were put into 10% v/v ethanol for 24 h to obtain extract solution and the used masses of all samples were listed in Table S2. 500 μL of sample was then mixed with 5.0 mL of ABTS working solution and incubated in the dark at room temperature for 6 min. The absorbance was recorded at 734 nm. The ABTS radical scavenging activity was calculated as follows:

$$\text{ABTS scavenging rate } (\%) = \frac{A_{Blank} - A_{Sample}}{A_{Blank}} \times 100\% \quad (6)$$

where A_{blank} is the absorbance of the ABTS solution mixed with 10% *v*/v ethanol, and A_{sample} is the absorbance of the ABTS solution mixed with the sample extract prepared in 10% v/v ethanol.

2.5. Statistical analysis

All experiments were conducted at least three times, and the results were expressed as mean value ± standard deviation. All data were analyzed by one-way analysis of variance (ANOVA) to determine the significance ($p < 0.05$) by IBM SPSS and plotted by Origin 2023.

3. Results and discussion

3.1. Effect of pH on the properties of the particles

The Z NPs prepared at pH 3–5 are presented in Fig. 2A. Z NPs formed when zein solution was dropped into deionized water due to hydrophobic interactions and hydrogen bonding [29]. All nanoparticles exhibited particle sizes below 120 nm with PDI < 0.20. The ζ potential of PUL and Z NPs were illustrated in Fig. 2B. Z NPs were positively charged at pH 3–5 and negatively charged at pH 6–8, since the isoelectric point (pI) of zein is around 6.2–6.8. PUL was negatively charged in all the tested conditions. PUL is a nonionic polysaccharide rather than a typical anionic polysaccharide containing strongly ionizable groups. Therefore, the negative ζ potential measured for PUL in the present study should be interpreted as an apparent surface charge under the experimental conditions, which may arise from interfacial ion adsorption and the solution environment [30,31]. The values of ζ potentials of PUL at pH 3 and 4 were under 10 mV, while at pH 5–8 then values were above 10 mV. The relatively lower ζ potential values of PUL at low pH may be related to changes in interfacial ion adsorption under acidic conditions [32]. In contrast, the higher ζ potential values observed at pH 5–8 suggested relatively better colloidal stability of the pullulan solution [33]. Electrostatic attractions occurred when two substances with opposite charges exist. Hence, at pH 3–5 for acidic conditions, positively charged Z NPs and negatively charged PUL would attract each other driven by electrostatic interactions, resulting in the deposition of a PUL outer layer on the surface of Z NPs to form pullulan-coated ZP NPs. As mentioned above, ζ potentials of PUL at pH 3 and 4 were not high enough to maintain the stable existence of PUL; therefore, even though the particle size of Z NPs at pH 5 was the largest, pH 5 was still selected as experimental condition for their preparation of ZP NPs, taking into account the results of ζ potential, particle size, and PDI.

3.2. Effect of zein/pullulan ratio

ZP NPs were prepared with different composite mass ratio of Z NPs and PUL. Fig. 3 shows the ζ potentials, particle size, PDI, and turbidity of different ZP NPs. With the addition of PUL, the ζ potential (Fig. 3A) changed from positive to negative and became stable when the composite mass ratio of Z NPs and PUL was 1:2, which could be attributed to the deposition of negatively charged PUL on the surface of positively charged Z NPs driven by electrostatic attraction [27]. For higher ratios, no significant changes were observed, suggesting that there is full coverage of PUL on the surface of the Z NPs.

Photos and turbidity of different ZP NPs are shown in Fig. 3B and Fig. S1. The changes in turbidity were monitored to evaluate the interactions between PUL and Z NPs [34]. It could be seen that when the mass ratio of zein to PUL was 3:1, 2:1, and 1:1, aggregation occurred between PUL and Z NPs, which was observed by the precipitation at the bottom. This is because the positive and negative charges in the whole system tend to be balanced, or Z NPs still dominated, leading to enhanced interactions between particles and aggregation to form precipitates [35]. When the amount of PUL added increased, the precipitation and aggregation did not occur and the whole system became stable. This may be due to the fact that when the amount of added PUL was sufficient, PUL formed a more complete coating layer, which increased the spatial hindrance between particles, preventing direct contact between particles, and reducing aggregation and precipitation [36]. At the same time, at pH 5, the deposited PUL layer likely contributed to electrostatic stabilization, that is, a combination of steric hindrance from the PUL coating and electrostatic repulsion between

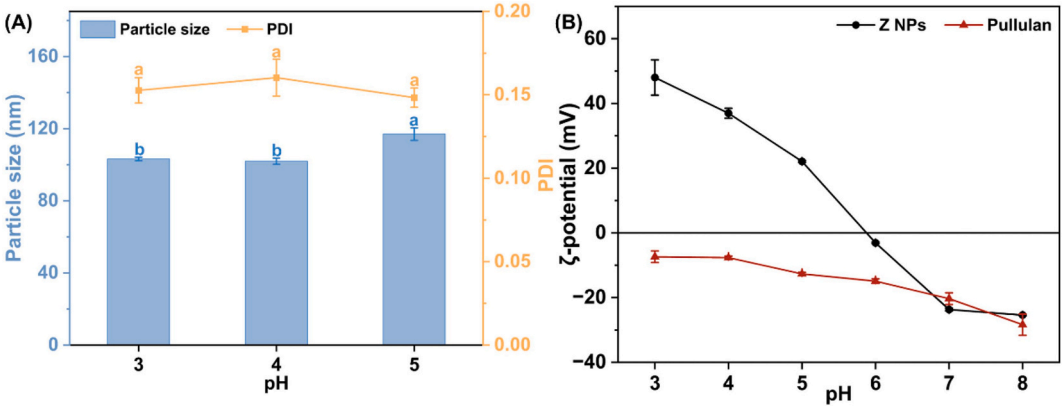

Fig. 2. Effect of pH on the physicochemical properties of Z NPs and pullulan. (A) Particle size and PDI of Z NPs at pH 3–5. (B) ζ potential of Z NPs and pullulan at pH 3–8.

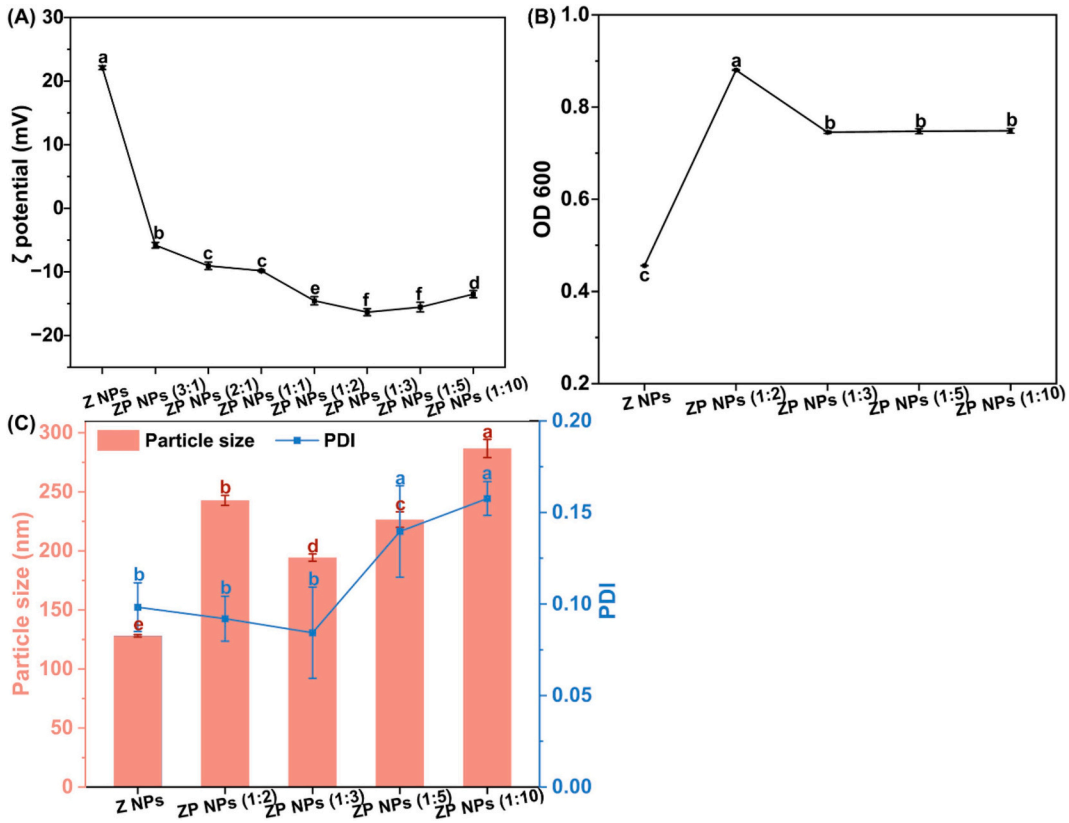

Fig. 3. Effect of the mass ratio of Z NPs to PUL on the properties of ZP NPs. (A) ζ potential, (B) turbidity, and (C) particle size and PDI of ZP NPs prepared at different Z NPs/PUL mass ratios.

negatively charged particles, thereby enhancing the stability of the solution. When the mass ratio of Z NPs to PUL reached 1:3, even if the amount of added PUL continued to increase, the turbidity still tended to stabilize and remained basically unchanged.

As for the particle size and PDI, all ZP NPs exhibited particle size below 300 nm with PDI below 0.20 (Fig. 3C). With PUL coated on the surface of Z NPs, all particle sizes increased compared to Z NPs, and the composite nanoparticles obtained had the smallest particle size when Z NPs and PUL were mixed with a mass ratio of 1:3. The particle size and PDI decreased first and then increased with the addition of PUL.

Two reasons contributed to the initial increase in particle size. One was the enhancement of hydrogen bonding and interparticle association, and the other was the incomplete coating of PUL on the surface of Z NPs. Due to the high hydroxyl content of PUL, it formed hydrogen bonds or weak electrostatic interactions with the surface of Z NPs. At low concentrations, PUL would absorb onto the surface of Z NPs, forming "bridging" that promoted particle aggregation [37–39]. At the same time, due to the low content of PUL, it could not completely coat the surface of Z NPs, which then led to the aggregation of some particles, resulting in an increase in particle size. When the concentration of PUL further increased, PUL and Z NPs could form a stable core-shell structure. The outermost PUL layer could provide strong electrostatic and spatial repulsion, suppress particle aggregation, and improve particle stability [37,40]. It should be noted that the increase in particle size after coating cannot be attributed solely to shell formation. A certain degree of particle association or loose aggregation might also have contributed to the enlarged particle size. In addition, the full particle size distribution profiles (Fig. S2) showed that both ZQ NPs and ZQP NPs mainly exhibited unimodal distributions, while the distributions of ZQP NPs were shifted toward larger particle sizes compared with the corresponding ZQ NPs. This result further supports that PUL coating increased the hydrodynamic diameter of the nanoparticles. Meanwhile, the slightly broader distributions observed for some ZQP NPs suggest that, besides surface coating, a certain degree of loose particle association might also have contributed to the increased particle size. However, if PUL was added in excess, bridging aggregation might occur between particles, resulting in particle aggregation and the increase in particle size [41]. Therefore, considering the particle size, potential and turbidity, the mass composite ratio of 1:3 between Z NPs and PUL was selected to prepare ZP NPs for subsequent experiments.

3.3. Encapsulation of Que in nanoparticles

Different masses of added Que were used to explore the optimal Que loading for Z NPs and ZP NPs. The particle size, PDI, and ζ potentials are illustrated in Fig. 4A and B. When zein-Que mixed solution was dropped into deionized water, due to the stronger hydrophobicity of Que compared to zein, Que was more easily encapsulated in the hydrophobic core formed by zein, resulting in a core-shell structure where Que was encapsulated internally and zein acted as a protective shell on the outside [42]. As the amount of Que added gradually increased, the particle size of ZQ NPs gradually decreased within an appropriate concentration range, suggesting the formation of more compact self-assembled particles. This may be because moderate amounts of Que interacted with zein and were incorporated into the hydrophobic domains of the nanoparticles during self-assembly, thereby promoting tighter molecular packing. At the same time, Que reduced the aggregation between ZQ NPs particles and achieved a reduction in particle size [43]. However, it was noteworthy that excessive Que led to saturation of zein's loading capacity for Que, resulting in the formation of unstable aggregates of excess Que on the particle surface, which were prone to hydrophobic interactions between particles [44]. Additionally, the dense structure between Que and Z NPs became looser or irregular, exacerbating the increase in particle size from 123.3 ± 0.15 nm to

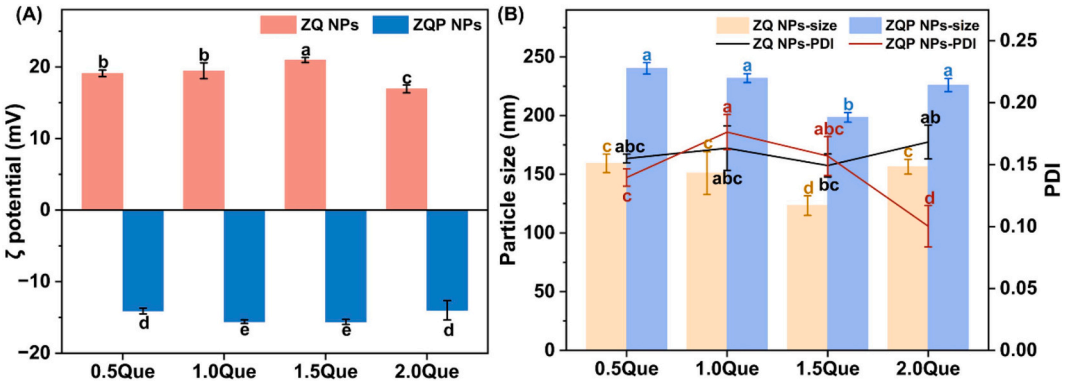

Fig. 4. Effect of Que addition amount on the physicochemical properties of ZQ NPs and ZQP NPs. (A) ζ potential, and (B) particle size and PDI.

156.43 ± 0.17 nm. For ZQP NPs, the particle size showed a similar trend to that of ZQ NPs, first decreasing and then increasing with the addition of Que with the smallest size of 198.47 ± 0.16 nm. For lower amounts of Que added, PUL uniformly deposited on the surface of dense ZQ NPs through electrostatic interactions, forming a dense shell layer. On the contrary, when Que was added to excess, unencapsulated Que occupied the surface of ZQ NPs, which may shield the positive charges on the zein core, thereby reducing the electrostatic attraction between ZQ NPs and negatively charged PUL, and leading to incomplete or uneven coating [44]. Therefore, the particle size became larger due to uneven coverage of PUL and bridging aggregation.

In the case of ζ potential, the absolute value of ZQ NPs and ZQP NPs first increased and decreased reaching a maximum value when Que was added at 1.5 mg/mL, which was 20.97 ± 0.35 mV for ZQ NPs and −15.63 ± 0.35 mV for ZQP NPs. Based on the denser structure of ZQ NPs resulting from the addition of Que, ZQ NPs became more stable, which led to an increase in the absolute value of ζ potential. When the excess Que formed a neutral or weak electric layer on the surface of ZQ NPs, the absolute value of ζ potential decreased due to the shielding of surface charges on zein. Similar principles could also be used to explain the changes in ζ potential of ZQP NPs. By enhancing surface smoothness, the lack of surplus Que improved PUL surface attachment to ZQ NPs, which meant that PUL could achieve full cover. Que on the surface of ZQ NPs restricted the adsorption of PUL, leading to a decrease in the absolute value of ζ potential.

EE and LC indicated the ability and efficiency of loading Que, which were illustrated in Table 1. EE increased with the addition of Que and reached a maximum when Que was added at 1.5 mg/mL. The observed result might be attributed to the different distribution states of Que in ZQ NPs and ZQP NPs. At an appropriate addition level, Que was more likely to be encapsulated within the nanoparticles, whereas excessive Que may have remained adsorbed on the particle surface rather than being incorporated into the inner structure. After the addition of PUL, the EE of ZQP NPs increased compared with ZQ NPs, which might be attributed to the shell protection effect [45]. The incorporation of PUL enables its binding to the surface of zein through electrostatic interactions and hydrogen bonding, thereby reducing the leakage and precipitation of Que and improving encapsulation efficiency of ZQP NPs.

However, the LC of ZQP NPs was significantly lower than that of ZQ NPs. This was mainly related to the introduction of PUL as an additional coating material during the preparation of ZQP NPs. Although PUL coating improved the retention of Que in the nanoparticle system and thus increased EE, it also increased the total mass of the composite nanoparticles. Since LC is calculated based on the mass ratio of encapsulated Que to the total mass of nanoparticles, the added PUL reduced the mass fraction of Que in the final ZQP NPs, resulting in lower LC values. Therefore, the increase in EE and the decrease in LC after PUL coating were not contradictory but reflected the improved retention of Que together with the dilution effect caused by the added coating material. In summary, the addition amount of Que was determined as 1.5 mg/mL for the following experiment.

Table 1
Encapsulation efficiency and loading capacity of ZQ NPs and ZQP NPs with different amounts of Que.

Samples	Encapsulation efficiency (%)	Loading capacity (%)
0.5-ZQ NPs	65.15 ± 0.18^{h}	1.589 ± 0.004^{e}
1.0-ZQ NPs	69.49 ± 0.21^{g}	3.309 ± 0.010^{c}
1.5 ZQ NPs	79.38 ± 0.10^{d}	5.538 ± 0.007^{b}
2.0 ZQ NPs	76.21 ± 0.08^{e}	6.928 ± 0.007^{a}
0.5-ZQP NPs	73.52 ± 0.17^{f}	0.457 ± 0.001^{g}
1.0-ZQP NPs	80.87 ± 0.05^{c}	0.998 ± 0.001^{f}
1.5 ZQP NPs	87.22 ± 0.10^{a}	1.605 ± 0.002^{e}
2.0 ZQP NPs	84.90 ± 2.35^{b}	2.071 ± 0.057^{d}

Uppercase letters $^{(a-h)}$ indicate significant differences ($p < 0.05$) based on one-way ANOVA analysis.

3.4. Micromorphology

The surface morphology of nanoparticles is shown in Fig. 5, among which, Fig. 5b displays magnified views of nanoparticles. It can be clearly seen that Z NPs exhibited a spherical structure due to the decrease of solubility when dropped into water [45]. When Que was added, ZQ NPs still maintained a spherical morphology, while the particle size increased. The particle boundaries became clearer, and the particle surface showed slight roughness or aggregation [43]. This could be attributed to the hydrophobic interaction between Que and Z NPs, which enhanced the encapsulation of Que and strengthened intermolecular interactions. These results were also consistent with the results of ζ potential and particle size. As for ZP NPs, nanoparticles still exhibited a spherical appearance. However, compared with Z NPs, the surface of ZP NPs appeared rougher, which may be due to the surface coating of PUL [46,47]. This also provided evidence for the successful deposition of PUL on the surface of Z NPs. The same trend can also be seen in SEM results of ZQP NPs. Compared with ZQ NPs, the surface of ZQP NPs appeared more irregular in the micrographs, which may be associated with the deposition of PUL on the particle surface. Electrostatic interactions and hydrogen bonding promoted the coating progress of PUL on Z NPs, contributing to the formation of a denser and more stable structure, which was manifested as a more compact and rougher surface morphology. In addition, the particle size distribution graphs are provided in Fig. S3 to further compare the size characteristics of different nanoparticles.

TEM images (Fig. 5c) further provided structural evidence for the morphology of nanoparticles. Compared with Z NPs, ZQ NPs showed a relatively darker inner contrast in the TEM images, which may be associated with the incorporation of Que into the zein-rich inner region and the resulting increase in internal density. More importantly,

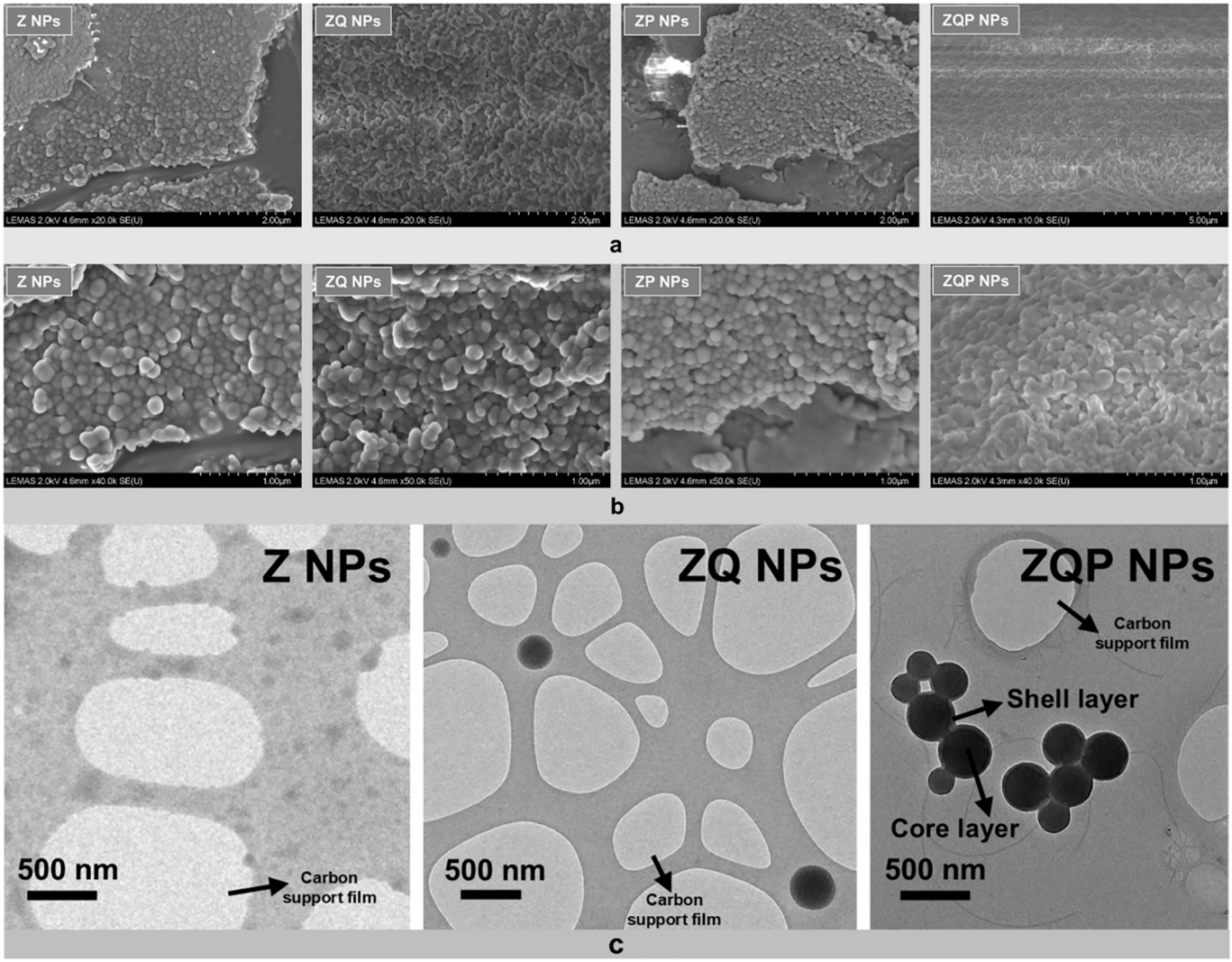

Fig. 5. SEM of different nanoparticles, from left to right: Z NPs, ZQ NPs, ZP NPs, and ZQP NPs. (a) Ordinary field of view and (b) magnified views. TEM of Z NPs, ZQ NPs, ZQP NPs (c).

compared with ZQ NPs, ZQP NPs exhibited a much more obvious boundary between the inner core (a gray and bounded interior) and outer shell (a light gray color shell), and a distinct core-shell-like structure could be clearly observed. Since Que was introduced during the anti-solvent self-assembly of zein, while PUL was deposited afterward as an outer coating layer, these results further supported that Que was predominantly incorporated into the inner hydrophobic domains of the nanoparticles, while PUL formed the outer shell layer on the particle surface.

3.5. Chemical structure and intermolecular interactions

The spectra of raw materials and samples are shown in Fig. 6A and B. For Z NPs, peaks at 3291 cm^{-1} represented the O—H stretching vibration and peaks at 2960–2920 cm^{-1} corresponded to the C—H stretching vibrations of alkane groups [17,42,48]. Meanwhile, peaks at 1642 cm^{-1} and 1527 cm^{-1} were dure to amide I bands (C═O stretching) and amide II bands (N—H bending coupled with C—N stretching), respectively [42]. When Que was encapsulated by zein nanoparticles, no characteristic peaks of Que were observed in ZQ NPs, which indicated that Que was completely encapsulated inside Z NPs [49]. Furthermore, after the addition of Que, peaks at 3291 cm^{-1} changed to 3295 cm^{-1}, owing to the hydrogen bonding interaction between zein and Que. The characteristic peaks at 2929 cm^{-1}, 1642 cm^{-1}, and 1527 cm^{-1} showed slight changes after Que encapsulation, with the amide II band shifting from 1527 cm^{-1} to 1523 cm^{-1}. Taken together, these spectral changes suggested that hydrophobic interactions were involved in the encapsulation of Que within Z NPs [17,50]. For pullulan, the peaks at 2924 cm^{-1} and 1638 cm^{-1} are associated with C—H stretching and H-O-H bending, respectively [51]. The peaks at 1230–1000 cm^{-1} are reflections of C-O-C stretching and C—O bonds [52,53] Moreover, the peak at 994 cm^{-1} represented the stretching vibration of C—O and peaks at 928 cm^{-1} and 848 cm^{-1} represented α-(1,6) glycosidic bonds and α-glucopyranoside units of pullulan [54,55].

At pH 5, Z NPs and ZQ NPs exhibited positive ζ potentials whereas PUL showed a slightly negative apparent ζ potential; therefore, electrostatic attraction occurred to contribute to complexation, alongside hydrogen bonding and hydrophobic associations of zein. When pullulan was added to Z NPs and ZQ NPs, peaks at 1527 cm^{-1} and 1523 cm^{-1} shifted to 1532 cm^{-1} and 1533 cm^{-1}, indicating hydrogen bonding between the amino groups of zein and the hydroxyl groups of PUL [48]. Meanwhile, weaker characteristic peaks of PUL could be observed in ZP NPs and ZQP NPs, probably because the strong absorption peak of zein masked part of the PUL signal. However, more obvious characteristic peaks were still observed at 1199 cm^{-1} and 1004 cm^{-1} compared with Z NPs and ZQ NPs. In addition, peaks at 1642 cm^{-1} and 1643 cm^{-1} shifted to 1645 cm^{-1} and 1646 cm^{-1}, respectively, supporting the occurrence of electrostatic interaction between zein and PUL. Similar spectral changes

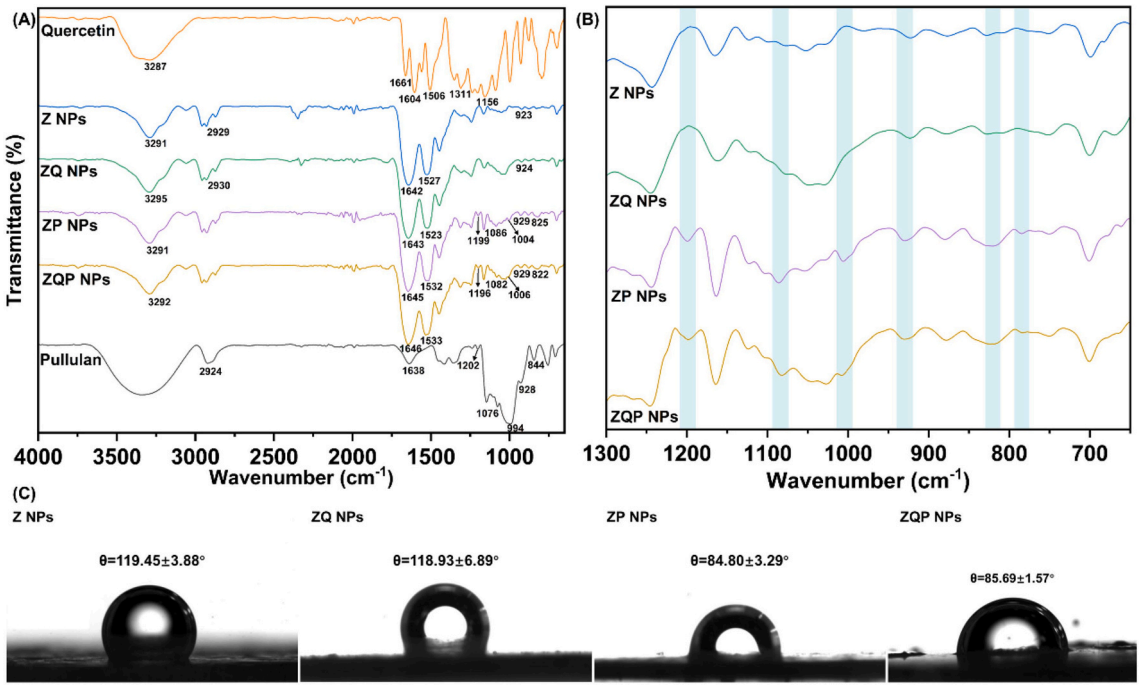

Fig. 6. The ATR-FTIR of raw materials and nanoparticles (A). Partially enlarged image of FTIR-ATR between 1300 and 650 cm^{-1} (B). The three-phrase water contact angle of nanoparticles (C).

have also been reported in pullulan-protein composite systems by Wang et al. [56]. The shifts in the amide bands after Que encapsulation and PUL coating suggested not only the occurrence of intermolecular interactions but also changes in the molecular environment of zein. This indicated that the incorporation of Que and the subsequent pullulan coating may have altered the packing state and local structural organization of the zein matrix, which was consistent with the observed changes in particle size, surface properties, and stability.

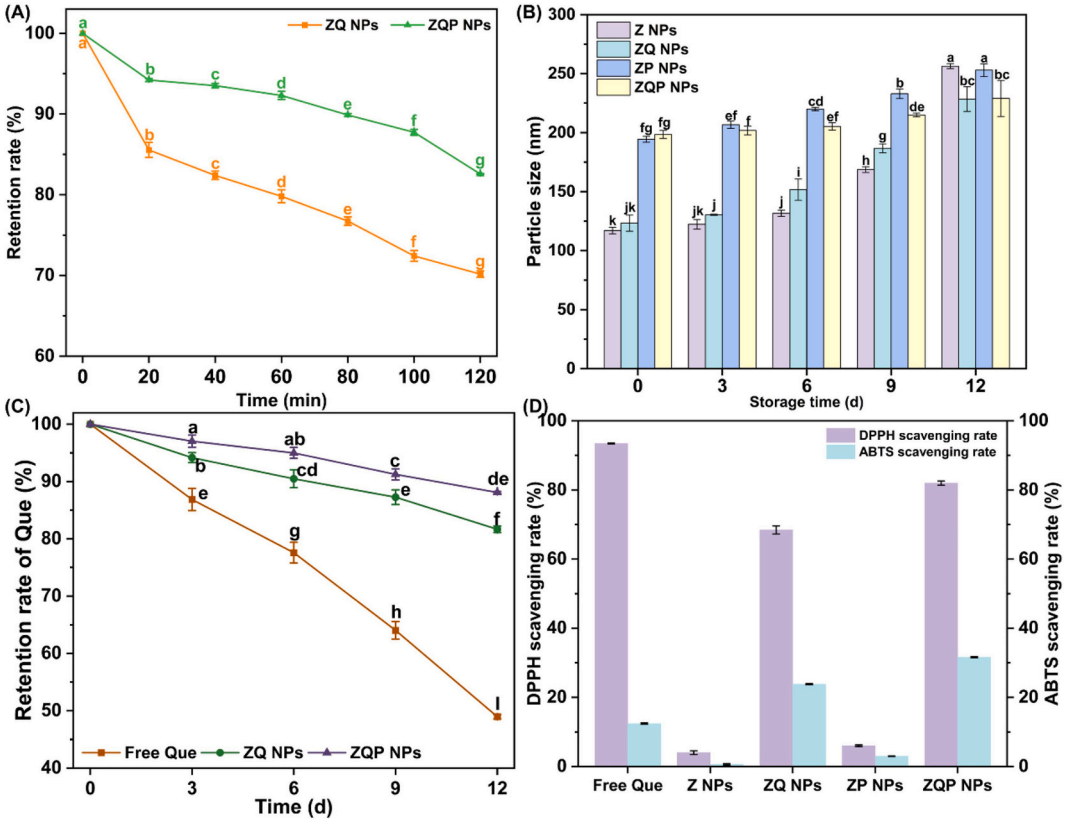

Fig. 7. The retention rate of ZQ NPs and ZQP NPs during heating treatment at 90 °C (A). Changes in particle size of nanoparticles during storage time (B). Retention rate of Que in Que-loaded nanoparticles during storage (C). The antioxidant ability of nanoparticles (D).

3.6. WCA

The WCA of nanoparticles is shown in Fig. 6C. The value of WCA is an effective manifestation of hydrophilicity and hydrophobicity. Typically, WCA $< 90°$ represented better affinity for water and showed hydrophilicity, while WCA $> 90°$ indicated better affinity for oil and showed hydrophobicity [57]. Since Z NPs and ZQ NPs were zein loaded on the outside, nanoparticles consequently exhibited hydrophobic characteristics based on the hydrophobic character of zein. When PUL were coated on the surface of Z NPs and ZQ NPs, due to the hydrophilicity of PUL, the WCA of ZP NPs and ZQP NPs became smaller and lower than 90°.

3.7. Thermal stability

Thermal stability of ZQ NPs and ZQP NPs was evaluated through the retention rate of Que. When high temperature was applied, Que would undergo degradation; therefore, the higher the retention rate of Que, the better the thermal stability of nanoparticles. As shown in Fig. 7A, the retention rate of ZQ NPs and ZQP NPs both decreased with the extension of heating time, especially during the first 20 mins, which could be related to the destruction of nanoparticle structures at the initial stage. In addition, this rapid decrease may also be attributed to the preferential degradation of Que located on or near the particle surface, or Que that was relatively loosely bound, while the more stably encapsulated Que in the inner region of the nanoparticles showed better resistance to thermal treatment. It should be noted that compared with ZQ NPs, ZQP NPs showed a lower degradation rate, resulting from the more stable structure formed by the PUL coated on the surface, which could promote the property of thermal-degradation resistance of nanoparticles [58]. Moreover, the retention rate of Que in ZQP NPs was always higher than that in ZQ NPs, indicating the protection effect of PUL for nanoparticles. When the heating progress came to an end at 120 mins, the retention rate of Que in ZQ NPs 70.18 ± 0.40% while it was 82.57 ± 0.07% in ZQP NPs, proving that PUL coating protected the Que from degradation during high temperature. Moreover, the sizes of ZQ NPs and ZQP NPs before and after heating were also compared and were shown in Fig. S4. Compared with ZQ NPs, the size changes of ZQP NPs after heating treatment were significantly smaller, which could also prove that the coating of PUL enhanced the thermal stability of Que-loaded nanoparticles.

3.8. Storage stability and photostability

The changes in particle size of Z NPs, ZQ NPs, ZP NPs and ZQP NPs were monitored over a 12-day storage period at 4 °C to assess their storage stability (Fig. 7B). All nanoparticles showed an upward trend in particle size as storage time increased, and Z NPs and ZQ NPs have the largest changes in particle size, increasing from 117.00 ± 2.83 nm and 123.33 ± 6.85 nm to 256.33 ± 2.05 nm and 228.43 ± 10.42 nm, respectively. In contrast, ZP NPs and ZQP NPs showed fewer significant changes in particle size, meaning that ZP NPs and ZQP NPs had better stability than Z NPs and ZQ NPs, which might be attributed to sufficient electrostatic repulsion to support spatial hindrance stability. Meanwhile, compared to the inherently hydrophobic zein, the coating with hydrophilic PUL transformed the surface properties of the nanoparticles from hydrophobic to hydrophilic, thus blocking the particle aggregation induced by hydrophobic effect. Similar results were obtained by J. Zhang et al. [42] when carboxymethyl starch was coated outside zein-gelatin nanoparticles. Meanwhile, although the particle sizes of ZP NPs and ZQP NPs also increased slightly during storage, the increase was much smaller than that of the uncoated nanoparticles, indicating that the PUL coating effectively slowed down particle growth rather than completely preventing it. This gradual increase in particle size may be related to weak interparticle association or very slow aggregation during storage, despite the steric barrier provided by the PUL layer. Notably, the relatively large error bars of Z NPs and ZQ NPs on day 12 suggest increased sample heterogeneity after prolonged storage, indicating reduced dispersion stability, possibly due to particle aggregation or structural instability.

The retention rate of free Que, ZQ NPs and ZQP NPs were also studied in Fig. 7C. After encapsulation, the degradation of Que was significantly improved during storage, as evidenced by the fact that only 48.96 ± 0.83% of free Que was preserved while the retention rates of Que in ZQ NPs and ZQP NPs were 81.67 ± 0.56% and 88.10 ± 0.16%, respectively. This resulted from the fact that by entrapping Que within nanoparticles, its interaction with the aqueous phase, where degradation reactions are typically accelerated, was effectively reduced [39]. When it comes to ZQ NPs and ZQP NPs, the retention rate of Que in ZQP NPs was higher than ZQ NPs, due to the protection effect of PUL on the surface of ZQ NPs.

Since Que is also susceptible to light-induced degradation, the photostability of ZQ NPs and ZQP NPs was further evaluated under light exposure (Fig. S5). After light treatment, ZQP NPs exhibited a higher retention rate of Que than ZQ NPs, indicating that the coating of PUL improved the light stability of Que-loaded nanoparticles. This might be because the outer PUL layer reduced the direct exposure of encapsulated Que to the external environment and thus provided additional protection against light-induced degradation. These results were consistent with the storage stability results, further confirming the protective effect of PUL coating on the stability of Que.

3.9. Antioxidant ability

The DPPH scavenging rate was used to assess the antioxidant ability of nanoparticles since Que has strong free radical scavenging ability. The results of DPPH scavenging rate are shown in Fig. 7D. It was obvious that Z NPs and ZP NPs showed extremely low antioxidant ability due to the lack of Que and the almost non-existent antioxidant properties of zein and PUL [42]. After the existence of Que, the antioxidant ability significantly increased, which was 68.41 ± 1.19% (ZQ NPs) and 81.96 ± 0.61% (ZQP NPs), respectively, confirming that Que was the main contributor to the radical scavenging activity. To ensure a fair comparison, ZQ NPs, ZQP NPs, and free Que were further compared at the same Que-equivalent amount. The results showed that free Que had the highest DPPH scavenging rate and ZQ NPs had the lowest value among three samples. For free Que, it was directly exposed to DPPH radicals in the solution, allowing more immediate interaction between Que and DPPH. In comparison, the lower activity of ZQ NPs was probably due to the partial encapsulation of Que within the ZQ NPs, which limited the direct accessibility of Que to DPPH radicals. Notably, ZQP NPs exhibited a higher scavenging rate than ZQ NPs even at the same Que-equivalent amount. This result may be attributed to the hydrophilic PUL coating, which improved the redispersibility and dispersion stability of nanoparticles. Better dispersion could increase the effective surface area available for radical scavenging. Moreover, PUL coating may also contribute to the stabilization of Que in the nanoparticle system, allowing more effective utilization of the encapsulated Que. Similar results have also been reported in other quercetin-loaded zein nanoparticles with polysaccharide-based surface modification, where the antioxidant activity of the nano system was retained after coating [59].

To provide a more application-relevant evaluation, the antioxidant activity of samples was further tested in 10% *v*/v ethanol food simulant by the ABTS radical scavenging assay under the same Que-equivalent conditions. For samples containing Que, ZQP NPs showed the highest ABTS scavenging rate in 10% v/v food simulant with 23.81 ± 0.15%, while free Que showed the lowest with 12.42 ± 0.19%. The extremely low antioxidant activity of Z NPs and ZP NPs further confirmed that Que was the main contributor to the radical scavenging activity of the system. Compared with free Que, both ZQ NPs and ZQP NPs exhibited higher ABTS scavenging activity, suggesting that nanoparticle incorporation improved the effective dispersion and utilization of Que in the

food simulant. More importantly, ZQP NPs showed a higher scavenging activity than ZQ NPs, indicating that the hydrophilic PUL coating further enhanced the dispersion stability of the nanoparticles in 10% v/v ethanol, thereby promoting the antioxidant performance of encapsulated Que. These results suggested that PUL coating not only improved the physicochemical stability of the nanoparticles but also contributed to better antioxidant functionality under a food-simulant-related condition.

4. Conclusion

In our study, Z NPs were successfully prepared by dropping zein solution into deionized water. This might be due to the spontaneous inward folding of hydrophobic regions, which contributed to the formation of a hydrophobic core. At the same time, the self-assembly of zein, driven by hydrophobic interactions and hydrogen bonding, facilitated the formation of a compact and stable nanoparticle core, which helped maintain structural integrity and prevented macroscopic aggregation. When Que was dispersed in zein solution and dropped into deionized water, due to the stronger hydrophobicity of Que than zein, Que was more easily encapsulated in the hydrophobic core formed by zein, resulting in a core-shell structure. The optimized ZQP NPs exhibited a spherical structure and had the highest Que encapsulation efficiency. Moreover, after surface coating with PUL, the thermal stability and storage stability of PUL-coated nanoparticles also improved because of the more stable structure formed by the PUL coating on the surface. The FTIR, thermal stability, and storage stability results suggested that PUL coating not only improved the physicochemical stability of the nanoparticles but also contributed to Que stabilization by providing additional surface protection. The DPPH scavenging ability also proved that both ZQ NPs and ZQP NPs had strong antioxidant activity. Overall, the encapsulation of Que within the zein core and the subsequent coating of PUL on the zein surface significantly enhance the hydrophilicity of the nanoparticles. These nanoparticles exhibit superior thermal stability and outstanding antioxidant capacity. This study demonstrates the feasibility of constructing ZQP NPs with improved water compatibility and storage-related stability. These findings support their potential as packaging-oriented antioxidant nanocarriers, providing a foundational step toward their future application in functional, water-soluble films, although further studies are still needed to validate their performance in specific film matrices and practical food packaging applications.

CRediT authorship contribution statement

Jialin Sun: Writing – review & editing, Writing – original draft, Software, Methodology, Formal analysis, Data curation. **Megan Povey:** Writing – review & editing, Supervision. **Wing-Fu Lai:** Writing – review & editing, Supervision. **Paraskevi Paximada:** Writing – review & editing, Supervision, Funding acquisition.

Declaration of competing interest

The authors declare that they have no known competing financial interests or personal relationships that could have appeared to influence the work reported in this paper.

Acknowledgments

This work was also supported by the China Scholarship Council (No. 202406330027).

Appendix A. Supplementary data

Supplementary data to this article can be found online at https://doi.org/10.1016/j.ijbiomac.2026.153600.

Data availability

Data will be made available on request.

References

[1] A. Mirzaei, Y. Bina Jorshari, S. Jananshir, M. Noori, M. Mahdavi, Colorimetric ph-sensitive hydrogel film based on kappa-carrageenan containing quercetin or eucalyptus leaf extract for freshness monitoring of chicken meat, Food Chem. X. 22 (2024) 101307, https://doi.org/10.1016/j.fochx.2024.101307.
[2] C. Yin, X. Ding, Z. Lin, J. Cao, W. Shi, J. Wang, D. Xu, D. Xu, Y. Liu, G. Liu, Preparation and characterization of quercetin@ZIF-L/GO@AgNPs nanocomposite film for room-temperature strawberry preservation, Food Chem. 450 (2024) 139411, https://doi.org/10.1016/j.foodchem.2024.139411.
[3] X. Chen, L. Zheng, B. Zhang, Z. Deng, H. Li, Synergistic protection of quercetin and lycopene against oxidative stress via SIRT1-Nox4-ROS axis in HUVEC cells, Curr. Res. Food Sci. 5 (2022) 1985–1993, https://doi.org/10.1016/j.crfs.2022.10.018.
[4] I.H. Elewi, N. Oladzadabbasabadi, M.F. Abbas, M.H. Al-Musawi, S. PourvatanDoust, H. Hajipour, M. Ghorbani, Encapsulation of cyclodextrin nanosponges containing quercetin in electrospun gelatin/kappa carrageenan nanofiber with antibacterial and antioxidant properties and their potential use for food packaging, LWT 233 (2025) 118525, https://doi.org/10.1016/j.lwt.2025.118525.
[5] W. Ji, M. Yang, Q. Li, J. Tuo, X. Chen, Formation and bioaccessibility of complexes of a quercetin-loaded preheated whey protein concentrate, LWT 220 (2025) 117581, https://doi.org/10.1016/j.lwt.2025.117581.
[6] D. Zhang, N. Bu, L. Zhou, L. Lin, Y. Wen, X. Chen, L. Huang, H. Lin, R. Mu, L. Wang, J. Pang, Quercetin-loaded melanin nanoparticle mediated konjac glucomannan/polycaprolactone bilayer film with dual-mode synergistic bactericidal activity for food packaging, Int. J. Biol. Macromol. 276 (2024) 133982, https://doi.org/10.1016/j.ijbiomac.2024.133982.
[7] I.G. Osojnik Crnivec, M. Skrt, T. Polak, D. Seremet, P. Mrak, D. Komes, U. Vrhovsek, N. Poklar Ulrih, Aspects of quercetin stability and its liposomal enhancement in yellow onion skin extracts, Food Chem. 459 (2024) 140347, https://doi.org/10.1016/j.foodchem.2024.140347.
[8] S. Dall'Acqua, G. Miolo, G. Innocenti, S. Caffieri, The photodegradation of quercetin: relation to oxidation, Molecules 17 (8) (2012) 8898–8907, https://doi.org/10.3390/molecules17088898.
[9] A. Kellil, S. Grigorakis, S. Loupassaki, D.P. Makris, Empirical kinetic modelling and mechanisms of quercetin thermal degradation in aqueous model systems: effect of pH and addition of antioxidants, Appl. Sci. 11 (6) (2021) 2579, https://doi.org/10.3390/app11062579.
[10] R. Zhao, S. Hu, T. Chen, Y. Li, X. Chi, S. Yu, W. Wang, D. Liu, B. Zhu, J. Hu, Innovative delivery strategies for quercetin: a comprehensive review of advances and challenges, Compr. Rev. Food Sci. Food Saf. 24 (3) (2025) e70146, https://doi.org/10.1111/1541-4337.70146.
[11] E. Mankan, C.Y. Karakas, O. Saroglu, M. Mzoughi, O. Sagdic, A. Karadag, Food-grade liposome-loaded delivery systems: current trends and future perspectives, Foods 14 (17) (2025) 2978, https://doi.org/10.3390/foods14172978.
[12] I. Tsichlis, V.D. Koufonikola, C. Chaikali, S. Hatziantoniou, C. Demetzos, A comparative study of the influence of lipid composition on stability, in vitro release, and antioxidant activity of quercetin-loaded ceramide-containing liposomes for topical delivery, AAPS PharmSciTech 26 (8) (2025) 1–13, https://doi.org/10.1208/s12249-025-03226-0.
[13] N. Sato, N. Shimizu, Subcritical solvent extraction and microencapsulation of flavonoids from onion skin waste, Appl. Food Res. 5 (2) (2025) 101391, https://doi.org/10.1016/j.afres.2025.101391.
[14] D. Nishimoto-Sauceda, L.E. Romero-Robles, M. Antunes-Ricardo, Biopolymer nanoparticles: a strategy to enhance stability, bioavailability, and biological effects of phenolic compounds as functional ingredients, J. Sci. Food Agric. 102 (1) (2022) 41–52, https://doi.org/10.1002/jsfa.11512.
[15] N.K. Hassan, M. Haider, J. Jagal, E. El-Labbad, I. Elsayed, M.S. Taha, Beta-cyclodextrin-capped self-sssembled zein nanoparticles for stable quercetin delivery, J. Drug Deliv. Sci. Technol. 111 (2025) 107174, https://doi.org/10.1016/j.jddst.2025.107174.
[16] Z. Wang, S. Ma, S. Chen, M. Deng, R. Peng, J. Xu, Z. Guo, Fabrication of glycosylated wheat gliadin hydrolysate nanoparticle for stabilization of quercetin: interaction characteristics, conformational changes and stability, Int. J. Biol. Macromol. 315 (Pt 1) (2025) 144481, https://doi.org/10.1016/j.ijbiomac.2025.144481.
[17] X. Xu, D. Dai, H. Yan, J. Du, Y. Zhang, T. Chen, Enhancing mechanical and blocking properties of gelatin films using zein-quercetin nanoparticle and applications for strawberry preservation, Food Chem. 464 (Pt 3) (2025) 141895, https://doi.org/10.1016/j.foodchem.2024.141895.
[18] Q. Liang, P. Cao, H. Lu, Y. Du, L. Kang, H. Ma, X. Ren, Ultrasonic engineering of zein-curcumin nanoparticles/sodium alginate composite films for active food packaging applications, Int. J. Biol. Macromol. 315 (Pt 2) (2025) 144268, https://doi.org/10.1016/j.ijbiomac.2025.144268.
[19] N. Sun, C. Chen, F. Zhu, Encapsulation of ferulic acid in quinoa protein and zein nanoparticles prepared through antisolvent precipitation: structure, stability and gastrointestinal digestion, Food Biosci. 68 (2025) 106760, https://doi.org/10.1016/j.fbio.2025.106760.
[20] L. Wei, J. Guo, X. Xu, H. Chen, Z. Zhang, Preparation and characterization of deep eutectic solvent-plasticized zein films embedded with cinnamaldehyde

nanoparticles and their application in the preservation of green oranges, LWT 238 (2025) 118865, https://doi.org/10.1016/j.lwt.2025.118865.
[21] T. Ghosh, R. Priyadarshi, C. Krebs de Souza, B.L. Angioletti, J.-W. Rhim, Advances in pullulan utilization for sustainable applications in food packaging and preservation: a mini-review, Trends Food Sci. Technol. 125 (2022) 43–53, https://doi.org/10.1016/j.tifs.2022.05.001.
[22] H. Li, D. Wang, C. Liu, J. Zhu, M. Fan, X. Sun, T. Wang, Y. Xu, Y. Cao, Fabrication of stable zein nanoparticles coated with soluble soybean polysaccharide for encapsulation of quercetin, Food Hydrocoll. 87 (2019) 342–351, https://doi.org/10.1016/j.foodhyd.2018.08.002.
[23] J. Lu, L. Xie, A. Wu, X. Wang, Y. Liang, X. Dai, Y. Cao, X. Li, Delivery of silybin using a zein-pullulan nanocomplex: fabrication, characterization, in vitro release properties and antioxidant capacity, Colloids Surf. B Biointerfaces 217 (2022) 112682, https://doi.org/10.1016/j.colsurfb.2022.112682.
[24] D. Zhang, F. Jiang, J. Ling, X.K. Ouyang, Y.G. Wang, Delivery of curcumin using a zein-xanthan gum nanocomplex: fabrication, characterization, and in vitro release properties, Colloids Surf. B Biointerfaces 204 (2021) 111827, https://doi.org/10.1016/j.colsurfb.2021.111827.
[25] A. Kaith, U. Garg, N. Jain, M. Pandey, S. Kaul, B. Gorain, M. Amin, Pullulan as a sustained release carrier for ocular drug delivery: a review, Int. J. Biol. Macromol. 309 (Pt 4) (2025) 143146, https://doi.org/10.1016/j.ijbiomac.2025.143146.
[26] Y. Zou, J. Ren, Y. Fan, Y. Cao, Y. Xie, X. Xiao, L. F., Enhanced hydrophobicity, antioxidant activity, and antimicrobial efficacy of edible starch-based films incorporating pullulan and geraniol for fresh salmon preservation, Food Packaging Shelf. 49 (2025) 101530, https://doi.org/10.1016/j.fpsl.2025.101530.
[27] W. Tao, I.M.P.L.V.O. Ferreira, J. He, V. de Freitas, N. Mateus, H. Oliveira, A. Fernandes, Tailored zein-polysaccharide nanoparticles for anthocyanin encapsulation: insights into preparation and characterization, Food Hydrocoll. 166 (2025) 111365, https://doi.org/10.1016/j.foodhyd.2025.111365.
[28] E. Apostolidis, A. Stergiou, D. Kioupis, A. Sadeghpour, P. Paximada, G. Kakali, I. Mandala, Production of nanoparticles from resistant starch via a simple three-step physical treatment, Food Hydrocoll. 137 (2023) 108412, https://doi.org/10.1016/j.foodhyd.2022.108412.
[29] X. Chen, K. Nie, L. Ma, X. Chen, Epicatechin gallate-mediated modulation of zein self-assembly and air-water interfacial properties of zein nanoparticles, Food Hydrocoll. 168 (2025) 111519, https://doi.org/10.1016/j.foodhyd.2025.111519.
[30] S. Barany, Polymer adsorption and electrokinetic potential of dispersed particles in weak and strong electric fields, Adv. Colloid Interface Sci. 222 (2015) 58–69, https://doi.org/10.1016/j.cis.2014.09.009.
[31] A. Luis, A. Ramos, F. Domingues, Pullulan films containing rockrose essential oil for potential food packaging applications, Antibiotics (Basel) 9 (10) (2020) 681, https://doi.org/10.3390/antibiotics9100681.
[32] R. Zimmermann, U. Freudenberg, R. Schweiß, D. Küttner, C. Werner, Hydroxide and hydronium ion adsorption - a survey, Curr. Opin. Colloid Interface Sci. 15 (3) (2010) 196–202, https://doi.org/10.1016/j.cocis.2010.01.002.
[33] S. Bhattacharjee, Dls and zeta potential - what they are and what they are not? J. Control. Release 235 (2016) 337–351, https://doi.org/10.1016/j.jconrel.2016.06.017.
[34] L. Wang, Z. Wei, C. Xue, Effect of carboxymethyl konjac glucomannan coating on the stability and colon-targeted delivery performance of fucoxanthin-loaded gliadin nanoparticles, Food Res. Int. 162 (Pt A) (2022) 111979, https://doi.org/10.1016/j.foodres.2022.111979.
[35] F. Ma, W. Lv, L. Wu, C. Duan, X. Li, D. Li, *Athyrium multidentatum* (doll.) ching polysaccharide coated zein nanoparticles for oral delivery of resveratrol: fabrication, characterization, stability and in vitro digestion, Food Biosci. 68 (2025) 106664, https://doi.org/10.1016/j.fbio.2025.106664.
[36] W. Wang, Y. Dai, C. Cheng, R. Wang, J. Ma, Q. Jing, Development and functional evaluation of curcumin-loaded zein-gum arabic-flaxseed gum complex nanoparticles for anti-fatigue applications, Int. J. Biol. Macromol. 310 (Pt 1) (2025) 142998, https://doi.org/10.1016/j.ijbiomac.2025.142998.
[37] L. Wu, Y. Jiang, C. Chen, W. Zhang, J. Guo, S. Liu, P. Wang, F. Ren, B. Xu, Y. Hu, Efficient stabilizing effect of low-dose zein/xanthan gum nanoparticles at the oil-water interface, Int. J. Biol. Macromol. 294 (2025) 139512, https://doi.org/10.1016/j.ijbiomac.2025.139512.
[38] Z. Zhang, Y. Meng, J. Wang, C. Qiu, W. Miao, Q. Lin, X. Li, S. Sang, D. J. McClements, A. Jiao, Z. Jin, Preparation and characterization of zein-based core-shell nanoparticles for encapsulation and delivery of hydrophobic nutrient molecules: enhancing environmental stress resistance and antioxidant activity, Food Hydrocoll. 148 (2024) 109524, https://doi.org/10.1016/j.foodhyd.2023.109524.
[39] Z. Zhang, Y. Hu, H. Ji, Q. Lin, X. Li, S. Sang, D. Julian McClements, L. Chen, J. Long, A. Jiao, X. Xu, Z. Jin, C. Qiu, Physicochemical stability, antioxidant activity, and antimicrobial activity of quercetin-loaded zein nanoparticles coated with dextrin-modified anionic polysaccharides, Food Chem. 415 (2023) 135736, https://doi.org/10.1016/j.foodchem.2023.135736.
[40] T. Zhang, S. Yu, X. Tang, C. Ai, H. Chen, J. Lin, H. Meng, X. Guo, Ethanol-soluble polysaccharide from sugar beet pulp for stabilizing zein nanoparticles and improving encapsulation of curcumin, Food Hydrocoll. 124 (2022) 107208, https://doi.org/10.1016/j.foodhyd.2021.107208.
[41] S. Liu, L. Yu, Y. Han, S. Wang, Z. Liu, H. Xu, Preparation, characterization, formation mechanism, and stability studies of zein/pectin nanoparticles for the delivery of prodigiosin, Int. J. Biol. Macromol. 290 (2025) 138915, https://doi.org/10.1016/j.ijbiomac.2024.138915.
[42] J. Zhang, C. Gan, K. Xu, H. Wang, H. Li, L. Yang, S. Sun, Fabrication and characterization of zein/gelatin/carboxymethyl starch nanoparticles as an efficient delivery vehicle for quercetin with improved stability and bioaccessibility, Int. J. Biol. Macromol. 308 (Pt 1) (2025) 142419, https://doi.org/10.1016/j.ijbiomac.2025.142409.
[43] Y. Zou, Y. Qian, X. Rong, K. Cao, D.J. McClements, K. Hu, Encapsulation of quercetin in biopolymer-coated zein nanoparticles: formation, stability, antioxidant capacity, and bioaccessibility, Food Hydrocoll. 120 (2021) 106980, https://doi.org/10.1016/j.foodhyd.2021.106980.
[44] Z. Yang, D.J. McClements, X. Peng, Z. Xu, M. Meng, L. Chen, Z. Jin, Fabrication of zein–carboxymethyl cellulose nanoparticles for co-delivery of quercetin and resveratrol, J. Food Eng. 341 (2023) 111322, https://doi.org/10.1016/j.jfoodeng.2022.111322.
[45] S. Chen, Y. Han, L. Jian, W. Liao, Y. Zhang, Y. Gao, Fabrication, characterization, physicochemical stability of zein-chitosan nanocomplex for co-encapsulating curcumin and resveratrol, Carbohydr. Polym. 236 (2020) 116090, https://doi.org/10.1016/j.carbpol.2020.116090.
[46] L. Chen, W. Xu, Z. Yang, D.J. McClements, X. Peng, Z. Xu, M. Meng, Y. Zou, G. Chen, Z. Jin, Co-encapsulation of quercetin and resveratrol: comparison in different layers of zein-carboxymethyl cellulose nanoparticles, Int. J. Biol. Macromol. 278 (Pt 2) (2024) 134827, https://doi.org/10.1016/j.ijbiomac.2024.134827.
[47] X. Zhang, X. Sun, Y. Chen, F. Zheng, H. Ban, J. Liu, D. Cai, L. Xiu, Study on the stability of sodium alginate modified zein/adzuki bean seed coat polyphenol composite nanoparticles and the loading of curcumin in emulsion, LWT 226 (2025) 117978, https://doi.org/10.1016/j.lwt.2025.117978.
[48] S. Amjadi, S. Gholizadeh, A. Ebrahimi, H. Almasi, H. Hamishehkar, R.A. Taheri, Development and characterization of the carvone-loaded zein/pullulan hybrid electrospun nanofibers for food and medical applications, Ind. Crop. Prod. 183 (2022) 114964, https://doi.org/10.1016/j.indcrop.2022.114964.
[49] W. Xu, D.J. McClements, Z. Zhang, R. Zhang, C. Qiu, J. Zhao, Z. Jin, L. Chen, Effect of tannic acid modification on antioxidant activity, antibacterial activity, environmental stability and release characteristics of quercetin loaded zein-carboxymethyl chitosan nanoparticles, Int. J. Biol. Macromol. 280 (Pt 2) (2024) 135853, https://doi.org/10.1016/j.ijbiomac.2024.135853.
[50] J. Yang, J. Xie, E. Paximada, Electrosprayed zein and quercetin particles: formation and properties, Food Bioproc. Tech. 18 (3) (2025) 2840–2853, https://doi.org/10.1007/s11947-024-03633-4.
[51] Z. Li, X. Wang, M. Zhang, H. He, B. Liang, C. Sun, X. Li, C. Ji, The loading of epigallocatechin gallate on bovine serum albumin and pullulan-based nanoparticles as effective antioxidant, Foods 11 (24) (2022) 4074, https://doi.org/10.3390/foods11245074.
[52] E. Celem, Z. Tarakci, Investigation of the use of fruit pomace and glycerol in the encapsulation of lactobacillus acidophilus (THT 030101) in pullulan-based electrospun nanofibers, Carbohydr. Polym. 356 (2025) 123341, https://doi.org/10.1016/j.carbpol.2025.123341.
[53] A. Tolun, M. Sharifuzzaman, Z. Altintas, Electrospun nanofibers of curcumin/hp-beta-cd/pullulan complex with enhanced solubility and controlled release in food and drug delivery applications, Int. J. Biol. Macromol. 300 (2025) 140064, https://doi.org/10.1016/j.ijbiomac.2025.140064.
[54] C. Chen, Y. Ding, Y. Sun, X. Li, C. Sun, F. Guo, X. Zeng, H. Gong, X. Fan, Chitosan/pullulan edible coatings containing thyme essential oil nanoemulsion: preparation, characterization and application in strawberry preservation, Int. J. Biol. Macromol. 309 (Pt 3) (2025) 143043, https://doi.org/10.1016/j.ijbiomac.2025.143043.
[55] S. Ji, W. Wang, L. Li, Q. Xia, Preparation and characterization of tamarind seed polysaccharide-pullulan sublingual films loaded with muco-inert nanoparticles for mucosal co-delivery of bsa and resveratrol, Carbohydr. Polym. 356 (2025) 123420, https://doi.org/10.1016/j.carbpol.2025.123420.
[56] Y. Wang, Z. Xie, H. Li, G. Zhang, R. Liu, J. Han, L. Zhang, Improvement in probiotic intestinal survival by electrospun milk fat globule membrane-pullulan nanofibers: fabrication and structural characterization, Food Chem. X. 23 (2024) 101756, https://doi.org/10.1016/j.fochx.2024.101756.
[57] R. Zhang, L. Li, C. Ma, F. Ettoumi, M. Javed, X. Lin, X. Shao, G. Xiao, Z. Luo, Shape-controlled fabrication of zein and peach gum polysaccharide based complex nanoparticles by anti-solvent precipitation for curcumin-loaded Pickering emulsion stabilization, Sustain. Chem. Pharm. 25 (2022) 100565, https://doi.org/10.1016/j.scp.2021.100565.
[58] H. Annappa, A. Tamatam, I. Nallamuthu, K. Ranganathan, Formulation of ph-responsive nanoparticles using zein/sodium alginate polymers for enhanced bioavailability of the vitamin D3, Int. J. Biol. Macromol. 313 (2025) 144140, https://doi.org/10.1016/j.ijbiomac.2025.144140.
[59] H. Lu, F. Mi, C. Chou, C. Lin, Y. Chen, C. Chu, C. Liu, Y. Lee, C. Shih, C. Cheng, Layer-by-layer assembly of quercetin-loaded zein/γPGA/low-molecular-weight chitosan/fucoidan nanosystem for targeting inflamed blood vessels, Int. J. Biol. Macromol. 267 (2024) 131369, https://doi.org/10.1016/j.ijbiomac.2024.131369.